NEURAL REGENERATION RESEARCH
www.nrronline.org

Research Article

Lactoferrin modification of berberine nanoliposomes enhances the neuroprotective effects in a mouse model of Alzheimer's disease

Lin Wang[1, #], Bi-Qiang Zhou[2, #], Ying-Hong Li[2], Qian-Qian Jiang[1], Wei-Hong Cong[3], Ke-Ji Chen[3, *], Xiao-Min Wen[4, *], Zheng-Zhi Wu[1, *]

https://doi.org/10.4103/1673-5374.344841
Date of submission: September 30, 2021
Date of decision: December 22, 2021
Date of acceptance: March 11, 2022
Date of web publication: June 6, 2022

From the Contents

Graphical Abstract

Lactoferrin modification of berberine nanoliposomes reduces Alzheimer's-like amyloid-β neurotoxicity through inhibiting AChE activity, Tau over-phosphorylation, and apoptosis

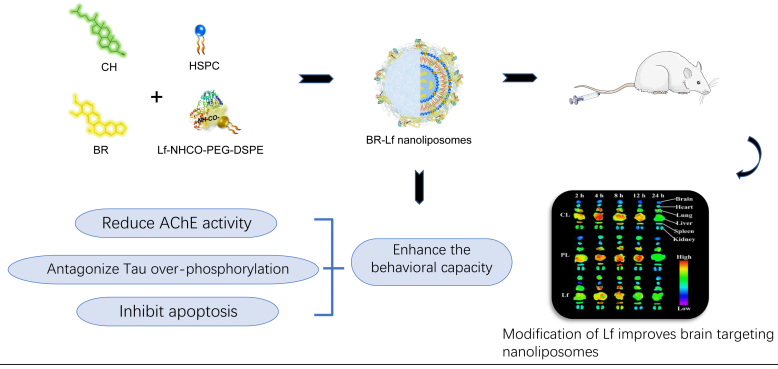

Abstract

Previous studies have shown that berberine has neuroprotective effects against Alzheimer's disease, including antagonizing tau phosphorylation, and inhibiting acetylcholinesterase activity and neural cell apoptosis. However, its low bioavailability and adverse reactions with conventional administration limit its clinical application. In this study, we prepared berberine nanoliposomes using liposomes characterized by low toxicity, high entrapment efficiency, and biodegradability, and modified them with lactoferrin. Lactoferrin-modified berberine nanoliposomes had uniform particle size and high entrapment efficiency. We used the lactoferrin-modified berberine nanoliposomes to treat a mouse model of Alzheimer's disease established by injection of amyloid-beta 1–42 into the lateral ventricle. Lactoferrin-modified berberine nanoliposomes inhibited acetylcholinesterase activity and apoptosis in the hippocampus, reduced tau over-phosphorylation in the cerebral cortex, and improved mouse behavior. These findings suggest that modification with lactoferrin can enhance the neuroprotective effects of berberine nanoliposomes in Alzheimer's disease.

Key Words: acetylcholinesterase; Alzheimer's disease; apoptosis; berberine; brain targeting; lactoferrin; nanoliposomes; neuroprotective effects; Tau phosphorylation

Introduction

Alzheimer's disease (AD) is a common neurodegenerative disorder, accounting for 60–80% of dementia cases worldwide, and its clinical symptoms mainly include progressive cognitive impairment, mnemonic trouble, language barriers, and personality changes (Gopalan et al., 2020). The available clinical drugs for AD are mainly acetylcholinesterase (AChE) inhibitors and glutamate receptor antagonists, which are only capable of relieving temporary clinical symptoms and fail to postpone or block the pathological course of AD. Furthermore, patients subjected to prolonged medication with these drugs often have difficulty tolerating them because of toxic side effects (Wang et al., 2018; Cummings et al., 2020). Therefore, there is an urgent need to improve conventional anti-AD drugs and develop new drugs for AD (Ballard et al., 2020; Cummings, 2021).

Berberine is a natural active ingredient extracted from rhizoma of Coptis chinensis. Its pharmacological action on the nervous system was initially reported in 1970 (Shanbhag et al., 1970). Evidence strongly supports that berberine has neuroprotective and substantial multi-target anti-AD pharmacodynamic effects, such as inhibiting AChE activity, antagonizing p-tau, and reducing neural cell apoptosis (Rahimi-Madiseh et al., 2017; Yuan et al., 2019; Imenshahidi and Hosseinzadeh, 2020). By reducing glycogen synthase kinase-3β activity and elevating protein phosphatase 2A activity in neurons, berberine inhibits tau over-phosphorylation at multiple sites and reduces neurofibrillary tangles to protect neural cells in the brain (Gong et al., 2006; Durairajan et al., 2012; Zhang et al., 2018). Berberine inhibits AChE, malondialdehyde, protein carbonyl activity, and DNA cleavage in hippocampus, increases anti-oxidative capacity, and improves spatial recognition memory in a mouse model of AD (de Oliveira et al., 2016; Sadraie et al., 2019). However, low bioavailability of berberine makes it difficult for a routine oral formulation to reach the effective drug concentration, and berberine's serious adverse reactions greatly impede its use for clinical application (Mirhadi et al., 2018; Song et al., 2020). Therefore, it is vital to use an effective drug carrier to minimize these limiting factors and enhance the efficacy of berberine (Raju et al., 2019).

Liposomes are a desirable drug carrier characterized by low toxicity, high entrapment efficiency, and biodegradability; furthermore, surface modification with polyethylene glycol can prolong the *in vivo* circulation duration of the drug (Pattni et al., 2015; Cai et al., 2022; Hernandez and Shukla, 2022). Wang et al. (2017) reported that compared with berberine solution, berberine liposomes were available at an appropriately high drug concentration to more efficiently inhibit tumor growth in mice. Allijn et al. (2017) demonstrated that entrapment with liposomes enabled high solubility of berberine, which effectively alleviated post-infarction cardiac insufficiency in mice. Calvo et al. (2020) demonstrated that use of berberine liposomes in visceral leishmaniasis prevented rapid hepatic metabolism of berberine and improved selective drug delivery to the infected organs. To the best of our knowledge, use of berberine liposomes in the prevention and treatment of AD has not yet been reported.

[1]The First Affiliated Hospital of Shenzhen University, Shenzhen Second People's Hospital, Shenzhen Institute of Geriatrics, Shenzhen, Guangdong Province, China; [2]The First Affiliated Hospital of Shenzhen University, Shenzhen Second People's Hospital, Shenzhen, Guangdong Province, China; [3]China Academy of Chinese Medical Sciences, Xiyuan Hospital, Beijing, China; [4]School of Chinese Medicine, Southern Medical University, Guangzhou, Guangdong Province, China
***Correspondence to:** Ke-Ji Chen, kjchenvip@163.com; Xiao-Min Wen, PhD, wxm@smu.edu.cn; Zheng-Zhi Wu, PhD, szwzz001@email.szu.edu.cn.
https://orcid.org/0000-0002-8819-609X (Zheng-Zhi Wu)
#These two authors contributed equally to this paper.

Funding: *This study was financially supported by Shenzhen Sanming Project of Medicine and Health, No. SZSM201612049 (to KJC); the Shenzhen Municipal Basic Research Project for Discipline Layout of China, No. JCYJ20170413161352000 (to YHL); and Guangdong Basic Research Project, No. 2020A1515011427 (to ZZW).*
How to cite this article: *Wang L, Zhou BQ, Li YH, Jiang QQ, Cong WH, Chen KJ, Wen XM, Wu ZZ (2023) Lactoferrin modification of berberine nanoliposomes enhances the neuroprotective effects in a mouse model of Alzheimer's disease. Neural Regen Res 18(1):226-232.*

A key issue of AD prevention and treatment with berberine liposomes is how to increase drug concentration at the lesion site in the brain. Modification with lactoferrin (Lf) is likely to solve this issue. Blood-brain barrier (BBB) endothelial cells express Lf receptors (LfR). Lf binding to LfR can mediate an Lf-modified drug carrier system through the BBB to increase drug concentration in the brain, and Lf has been widely applied in targeted nanotherapy for nervous system disorders (Huang et al., 2007; Yan et al., 2018; Mittal et al., 2020).

Liu et al. (2017) found that Lf-modified daunorubicin and magnolol liposomes were transported via the BBB and promoted drug accumulation in brain tumor tissue. Karami et al. (2019) showed that Lf-modified Indinavir nanoemulsion enhanced the brain permeation of Indinavir remarkably. Huang et al. (2013) reported that Lf modification of 99mTc labeled N,N-bis(2-mercaptoethyl)-N′,N′-diethylethylenediamine-entrapped liposomes increased *in vitro* cell uptake by a factor greater than three and increased brain uptake by a factor of two compared with non-modified liposomes. In this study, we used PEGylated nanoliposomes as drug carriers with Lf for brain-targeting modification, and successfully prepared PEGylated berberine hydrochloride (BR) nanoliposomes with brain-targeting function. The neuroprotective mechanism of berberine nanoliposomes on the behavioral capacity of a mouse model of AD-like amyloid β (Aβ) neurotoxicity was explored.

Methods

Preparation of BR nanoliposomes

Preparation of blank nanoliposomes

The blank nanoliposomes were produced using modified ethanol (Ante Biochemistry Co., Ltd., Suzhou, Anhui Province, China) injection. The membrane materials listed in **Table 1** were mixed with ethanol 10% (v/v) and then heated in a water bath at 65°C. $(NH_4)_2SO_4$ solution preheated to the same temperature was added to each vial, which was then stirred in a water bath for 20 minutes. The preliminary products were further processed by an ultrasonic cell disruptor (JY92-II, Scientz Biotechnology Co., Ltd., Ningbo, Zhejiang Province, China) and granulated by passing through 0.8, 0.45, and 0.22 μm microporous filters sequentially, resulting in suspensions of blank nanoliposomes (CL), PEGylated blank nanoliposomes (PL), and carboxyl-containing PEGylated blank nanoliposomes (PL-COOH), respectively.

Table 1 | **Basic formulations of blank nanoliposomes**

	CL	PL	PL-COOH
HSPC (mg)	150	150	300
CH (mg)	50	50	100
$mPEG_{2000}$-DSPE (mg)	–	50	30
DSPE-PEG_{2000}-COOH (mg)	–	–	60

CH: Cholesterol; CL: common blank nanoliposomes; DSPE-PEG_{2000}-COOH: dsteeyl phosphatidylethanolamine polyethylene glycol 2000-carboxyl; HSPC: hydrogenated soybean lecithin; $mPEG_{2000}$-DSPE: polyethylene glycol monoethyl ether 2000-disorieyl phosphatidylethanolamine; PL: PEGylated blank nanoliposomes; PL-COOH: carboxyl-containing PEGylated blank nanoliposomes.

Preparation of BR-CL, BR-PL and BR-PL-COOH

The blank nanoliposomes suspension was loaded into the top of a G100 column (Yuanye Biological Technology Co., Ltd., Shanghai, China) and centrifuged at 1500 × *g* for 4 minutes. Then, double-distilled water was added from the column top, and the column was centrifuged and eluted three times. The eluates were combined and mixed well to yield a liposome suspension having an $(NH_4)_2SO_4$ transmembrane ion gradient. Desired amounts of gradient liposomes CL, PL, and PL-COOH were collected, into which BR (purity > 98%, Meilun Bio. Co., Ltd., Dalian, Liaoning Province, China) solution was added at a drug-to-liposomes ratio of 1:20 (w/w). The solution was then incubated at 55°C for 15 minutes. Subsequently, drug loading was terminated in an ice water bath. BR common nanoliposomes (BR-CL), BR PEGylated nanoliposomes (BR-PL), and BR-PL-COOH were obtained, respectively.

Preparation of BR-Lf nanoliposomes

Unentrapped free drug in BR-PL-COOH nanoliposomes was removed by passing the liposomes through a dextran gel Sephadex G-100 column. Then, 1 mL of the liposomes (1 μmol -COOH) was accurately pipetted into a 10 mL vial, into which 0.5 mL of aqueous solution of N-(3-dimethylaminopropyl)-N-ethylcarbodiimide HCl (20 μmol) and 0.5 mL of aqueous solution of N-hydroxysuccinimide (10 μmol) were added in an ice water bath, and activated by magnetic stirring for 30 minutes. Subsequently, the ice water bath was removed, the reaction system returned to room temperature, and 6 mg of Lf (Japan Wako Pure Chemical Industries Ltd., Osaka, Japan) was added. After Lf was fully dissolved, 1.4 μL (0.4 μmol) of triethylamine was added. After 4 hours, an ice water bath was applied to stop the reaction, resulting in Lf-modified PEGylated BR nanoliposomes (BR-Lf).

Preparation of 1,1′-dioctadecyl-3,3,3′,3′-tetramethylindotricarbocyanine iodide nanoliposomes

Using the ethanol injection method (Jaafar-Maalej et al., 2010), 1,1′-dioctadecyl-3,3,3′,3′-tetramethyl-indotricarbocyanine iodide (DiR; AAT Bioquest Inc., Sunnyvale, CA, USA) nanoliposomes were prepared, including DiR common nanoliposomes (DiR-CL) and DiR PEGylated nanoliposomes (DiR-PL and DiR-PL-COOH). The membrane material shown in **Table 2** was dissolved in ethanol at 60°C. Some ethanol was evaporated. Then the hydration medium was poured into the remaining ethanol. Lf was conjugated to the surface of DiR-PL-COOH nanoliposomes, resulting in preparation of Lf-modified DiR PEGylated nanoliposomes (DiR-Lf).

Table 2 | **Basic formulations of DiR nanoliposomes**

	Formulations		
Liposomal composition	**DiR-CL**	**DiR-PL**	**DiR-Lf**
DiR (mg)	0.3	0.3	0.3
HSPC (mg)	30.0	30.0	30.0
CH (mg)	10.0	10.0	10.0
$mPEG_{2000}$-DSPE (mg)	–	11.4	3.0
DSPE-PEG_{2000}-COOH (mg)	–	–	6.0
H_2O (mL)	4	4	4

CH: Cholesterol; CL: common blank nanoliposomes; DiR: 1,1′-dioctadecyl-3,3,3′, 3′-tetramethyl-indotricarbocyanine iodide; DiR-CL: DiR common nanoliposomes; DiR-Lf: DiR PEGylated nanoliposomes with Lf modified; DiR-PL: DiR PEGylated nanoliposomes; DSPE-PEG_{2000}-COOH: dsteeyl phosphatidylethanolamine polyethylene glycol 2000-carboxyl; HSPC: hydrogenated soybean lecithin; Lf: lactoferrin; $mPEG_{2000}$-DSPE: polyethylene glycol monoethyl ether 2000-disorieyl phosphatidylethanolamine; PL: PEGylated blank nanoliposomes.

Characterization of BR nanoliposomes

Particle size and morphology

Nicomp-380 particle size analyzer (American Particle Sizing Systems Co., Ltd., San Francisco, CA, USA) was used to determine the liposomes particle size. Liposomal microstructure was examined under a transmission electron microscope (JM-1200EX, JEOL Ltd., Tokyo, Japan).

Entrapment efficiency

BR entrapment efficiency was determined by ultraviolet (UV) spectrophotometry (Luo et al., 2013). Samples (0.1 mL) of each BR nanoliposomes were collected in duplicate. One sample was diluted with methanol to 10 mL to disrupt the nanoliposomes, and then its absorbance at 420 nm was determined using a UV spectrophotometer (UV5100, Wanyi Science and Technology Co., Ltd., Hefei, Anhui Province, China), denoted as Atot. The other sample was loaded onto the top of a cation exchange fiber column, and centrifuged at 1500 × *g* for 4 minutes. Double-distilled water was added, and the resulting mixture was centrifuged at 1500 × *g* for 4 minutes. This step was repeated three times. Eluates were diluted with methanol to 10 mL to disrupt the liposomes. UV spectrophotometry was performed. The absorbance value was recorded as Alip. BR entrapment efficiency was calculated using the following formula:

$$EE\% = \frac{A_{lip}}{A_{tot}} \times 100\% \quad (1)$$

Grafting ratio of Lf in BR-Lf

Lf grafting ratio was determined by Coomassie brilliant blue method (Han et al., 2010). BR-Lf reaction solution (0.1 mL) was collected in duplicate. One sample was passed through dextran gel Sephadex G-100 column to remove unreacted Lf, and the second sample did not pass through the column. Specifically, 5 mL of acidic Coomassie brilliant blue G250 chromogen solution was added to 0.1 mL of BR-Lf. Absorbances A1 and A2 at 595 nm were determined using a UV spectrophotometer. Lf grafting ratio was calculated using the formula:

$$Lf_{grafted} = \frac{A_1}{A_2} \times 100\% \quad (2)$$

Establishment of a mouse model of AD-like Aβ neurotoxicity

Ninety-nine male healthy ICR mice (23–25 g, 2 months old, Liaoning Changsheng Biotechnology Ltd., Benxi, Liaoning Province, China, license No. SCXK (Liao) 2020-0001) were maintained at 25 ± 1°C in a 12-hour dark/light cycle with free access to food and drinking water. Mice were housed with no more than five per cage. To eliminate the potential influence of estrogen on the neuroprotective effect of berberine (Tang et al., 2018), only male rats were used in this study. This experiment was approved by the Institutional Animal Care and Use Committee of Shenyang Pharmaceutical University on August 24, 2020 (approval No. SYPH-IACUC-C2020-8-24-112). All experiments were designed and reported in accordance with the Animal Research: Reporting of *In Vivo* Experiments (ARRIVE) guidelines (Percie du Sert et al., 2020).

To perform behavioral tests and to investigate the mechanisms underlying neuroprotective effects, 54 mice were randomly divided into six groups (n = 9 per group): sham control (vehicle-injected), model (Aβ-injected), BR solution (Aβ + BR-S), BR-CL (Aβ + BR-CL), BR-PL (Aβ + BR-PL), and BR-Lf (Aβ + BR-Lf) groups. To perform fluorescence imaging, 45 mice were randomly divided into three groups (n = 15 per group): DiR-CL (Aβ + DiR-CL), DiR-PL (Aβ + DiR-PL), and DiR-Lf (Aβ + DiR-Lf) groups.

The mouse model of AD-like Aβ neurotoxicity was established by injection of Aβ-protein fragment 1–42 ($Aβ_{1–42}$) into the lateral ventricle (Goswami et al., 2020). $Aβ_{1–42}$ (0.1 mg; Sigma-Aldrich, St. Louis, MO, USA) was dissolved with 1.2 μL of dimethyl sulfoxide. Then, 161 μL of normal saline was added and the solution was incubated at 37°C for 120 hours and kept for later use. Each mouse was anesthetized with 2.5% avertin (240 mg/kg; Sigma-Aldrich) by

intraperitoneal injection. Fur was removed from the cranial incision region, the cranial skin was disinfected with alcohol and incised, and the skull was fixed to a brain stereotaxic apparatus (NARISHIGE SR-5N, Tokyo, Japan). The position of the lateral ventricle was determined according to a mouse brain stereotaxic map (left lateral ventricle: 0.5 mm away from the back of anterior fontanel, 1.1 mm left of the sagittal suture, and 3.0 mm below the skull surface) (Ji et al., 2014). Then, 3 μL of $A\beta_{1-42}$ solution (containing 410 pmol $A\beta_{1-42}$) or vehicle (normal saline for sham group) was perpendicularly injected with a microinjector (Hamilton, Bonaduz, Switzerland) using a 3-minute slow push followed by a 3-minute indwelling. Benzylpenicillin sodium was injected for anti-infection treatment.

Fluorescence imaging

Fluorescence imaging was used to observe the distribution of different DiR nanoliposomes in the model mice and evaluate their brain targeting. Immediately after the models were established, mice received a single injection of DiR-CL, DiR-PL, or DiR-Lf at a dose of 2.0 mg/kg (based on DiR) via the caudal vein. At 2, 4, 8, 12, and 24 hours after the injection, the mice were examined with an *in vivo* small animal imaging system (Bruker, Billerica, MA, USA), and both fluorescence and white light images were taken. After photography at each time point, three mice were sacrificed by cervical dislocation, and the brains, hearts, lungs, livers, spleens, and kidneys were then isolated and photographed under a fluorescence microscope. The molecular imaging software supplied with the system was used to quantitatively analyze near-infrared fluorescence intensity of the brain *ex vivo*.

Behavioral capacity tests

Different BR preparations (10 mg/kg) or vehicle (normal saline, 0.1 mL/10 g) were injected into mice by intravenous injection once every other day, starting on the day of the Aβ injection, for a total of seven doses.

The Y-maze test

To assess the effects of different BR preparations on spatial recognition memory of mice, we performed a Y-maze test (Bai et al., 2019). The Y-maze test apparatus (made by Shenyang Pharmaceutical University) was composed of three arms at an angle of 120° between adjacent arms, referred to as arms A–C. After completion of adaptive training, each animal was placed at the end of arm A and was allowed to visit the three arms freely. The total number of entries in the three arms within 5 minutes (N) and the sequence of arm entries were recorded. Successive entries in three different arms were counted as one correct alternation, and the number of correct alternations (N_s) was recorded. Throughout the testing, excreta were cleaned in time to eliminate remaining odor. Spontaneous alternation behavior was used to assess spatial working memory capacity of each mouse and was calculated using the following formula:

$$\text{Alternation behavior (\%)} = \frac{N_s}{N-2} \times 100\% \quad (3)$$

Novel object recognition test

To assess the effects of different BR preparations on learning and memory ability of mice, we performed a novel object recognition test after the Y-maze test (Jin et al., 2016). Two identical objects (A_1 and A_2) were placed at the same distance from the margin of an open field. An adapted mouse was put at any position with equal distances from both objects. The time that the mouse explored each object within 5 minutes was recorded. Then, the mouse was returned to its cage. One hour later, either of the objects was replaced by a totally different new object B, the mouse was put in the apparatus again, and the time that each object was explored within 5 minutes (t_{A1} and t_B) was recorded. Twenty-four hours later, the object B was replaced by a totally different object C, the mouse was once again put into the apparatus, and the time that each object was explored within 5 minutes (t_{A1} and t_C) was recorded. Preference indices for the novel objects were calculated using the following formulas, respectively:

$$\text{Preferential index (1 h)} = \frac{t_B}{t_{A_1}+t_B} \times 100\% \quad (4)$$

$$\text{Preferential index (24 h)} = \frac{t_C}{t_{A_1}+t_C} \times 100\% \quad (5)$$

Exploration into mechanism of neuroprotective effects

Harvesting

After the behavioral tests, the mice were put into a closed glass container with 4% ether solution for anesthesia. Four mice in each group were perfused to harvest their brains. The brains were fixed with 4% paraformaldehyde in a refrigerator at 4°C for 48 hours, dehydrated with alcohols at varying concentrations, hyalinized with xylene, waxed, and embedded for immunohistochemistry. For the remaining five mice, brain tissues were harvested without perfusion. Blood spots were blotted with filter paper on an ice box to remove blood from the brain, and immediately the hippocampus and cortex were isolated and transferred into an epoxy tube, which was then quickly frozen in liquid nitrogen and stored at –80°C. The frozen hippocampal tissue was selected at random for use in experiments.

AChE activity in mouse hippocampal tissue

Frozen hippocampal tissue from each group (n = 4 per group) was collected and tissue lysis buffer (5 μL of phenylmethylsulfonyl fluoride was added into every 1 mL of lysis buffer) was added at a ratio of 1:10 (10 μL/mg tissue). Under the cryogenic condition, an ultrasonic cell disruptor (Scientz) was used to prepare tissue homogenate. The tissue homogenate was placed in an ice bath for 1 hour, and was then centrifuged at 9000 × g at 4°C for 20 minutes. Then, the supernatant was collected and assayed according to the manufacturer instructions (Jiancheng Bioengineering Institute, Nanjing, Jiangsu Province, China). A standard tube, a blank tube, a control tube, and a test tube were used, in which the samples were mixed well and allowed to stand for 15 minutes. Then, 200 μL of each sample was pipetted into a 96-well plate. The optical density (OD) value of each well at 412 nm wavelength was determined by a plate reader (Thermo Fisher Scientific, Waltham, MA, USA). AChE activity in the tissue was calculated using the following formula. The protein concentration of the standard and test samples was detected by a bicinchoninic acid protein assay kit (Beyotime Biotechnology, Shanghai, China).

$$\text{AChE activity} = \frac{OD_{Test} - OD_{Control}}{OD_{Standard} - OD_{Blank}} \times \frac{C_{Standard}}{C_{Test}} \quad (6)$$

Tau phosphorylation in the mouse cerebral cortex

Expression of p-tau at Ser396 in the mouse cerebral cortex was examined by immunohistochemistry assay. Whole brains from each group (n = 4 per group) were routinely processed for paraffin embedding and cut into 5-μm-thick sections. The sections were dewaxed and hydrated. After antigen retrieval with citrate, endogenous peroxidases were blocked with hydrogen peroxide. Then, the sections were incubated with 5% bovine serum albumin blocking solution (Boster, Wuhan, Hubei Province, China) in a wet box at room temperature for 30 minutes. The surplus liquid was removed and the sections were not washed. The sections were incubated with rabbit monoclonal anti-Tau (phospho S396) (1:200, Abcam, Boston, MA, USA, Cat# ab32057, RRID: AB_778254) overnight at 4°C. After three washes with phosphate buffered solution (PBS) for 5 minutes each, the sections were incubated with horseradish peroxidase-labeled goat anti-rabbit IgG (1:5000, Boster, Cat# BA1055, RRID: AB_2734136) for 30 minutes at room temperature. After three washes with PBS for 5 minutes each, 50 μL of diaminobenzidine working solution was added dropwise until the brain section appeared pale brown. Subsequently, the sections were rinsed with tap water for 8 minutes, counterstained with hematoxylin, differentiated with hydrochloric acid-ethanol, dehydrated, and mounted on slides. Under a microscope (DS-Ri2, Nikon Corporation, Tokyo, Japan), the region of interest was examined and labeled cells per mm^2 were analyzed by ImageJ software (v1.8.0; National Institutes of Health, Bethesda, MD, USA) (Schneider et al., 2012).

Apoptosis in the mouse hippocampal tissue

The activity of pro-apoptotic factors caspase-3 and caspase-9 in hippocampal tissue of each group (n = 4 per group) were measured using caspase-3 and caspase-9 activity assay kits (Beyotime Biotechnology, Cat# C1116 and C1158, respectively). The hippocampal tissue was incubated at 37°C for 60 minutes and the OD value at 405 nm wavelength was determined by the plate reader. Caspase-3 and caspase-9 activity were calculated relative to the sham group.

Western blot assay was performed in three animals per group to measure the expression levels of Bax and Bcl-2 protein in hippocampal tissue. The concentration of bicinchoninic acid protein in the mouse hippocampus was determined. Protein samples (40 μg per group) were loaded and subjected to electrophoretic separation by sodium dodecyl sulfate-polyacrylamide gel electrophoresis. Then the protein was electrotransferred onto polyvinylidene difluoride (PVDF) membranes with a pore size of 0.45 μm. The membranes were placed into 5% skimmed milk powder (blocking buffer) (Yili, Hohhot, Inner Mongolia Autonomous Region, China), and gently shaken at room temperature in a shaker for 2 hours. The blocking buffer was used to prepare primary antibodies rabbit monoclonal anti-Bcl-2 (1:1000, Abcam, Cat# ab182858, RRID: AB_2715467) and rabbit polyclonal anti-Bax (1:1000, Proteintech, Wuhan, Hubei Province, China, Cat# 50599-2-Ig, RRID: AB_2061561). The protein side of the membrane was faced downward in full contact with the primary antibody, and was incubated in a refrigerator (Haier, Qingdao, Shandong Province, China) at 4°C overnight. The PVDF membranes were washed with PBS three times for 10 minutes each and were then incubated with secondary antibodies goat anti-mouse IgG (H+L) (1:5000, Thermo Fisher Scientific, Cat# 31460, RRID: AB_228341) and goat anti-rabbit IgG (H+L) (1:5000, Thermo Fisher Scientific, Cat# PA1-28555, RRID: AB_11009261) at room temperature for 2 hours. Then the membranes were washed with PBS three times for 10 minutes each. Immunoreactivity was detected with a highly sensitive luminescence reagent (Beyotime Biotechnology). The membranes were transferred into a gel imaging analyzer (Bio-Rad, Hercules, CA, USA) for exposure and development. The images were analyzed by IPP image analysis software (Media Cybernetics, Houston, TX, USA). Target protein expression was determined with β-actin (mouse monoclonal antibody, 1:1000, Santa Cruz Biotechnology Co., Ltd., Dallas, TX, USA, Cat# sc-47778, RRID: AB_2714189) as an internal reference.

Statistical analysis

No statistical methods were used to predetermine sample sizes. However, our sample sizes were similar to those reported in previous publications (Chen et al., 2017; Bai et al., 2019). No animals or data points were excluded from the analysis. Data were statistically analyzed using one-way analysis of variance followed by least significant difference *post hoc* test, with the exception of the fluorescence imaging data, which were analyzed using two-way analysis of variance followed by Duncan's multiple range test, in SPSS 21.0 software for Windows (IBM, Armonk, NY, USA). Experimental data were expressed as mean ± standard deviation (SD), and $P < 0.05$ was considered statistically significant.

Results

Characterization of BR nanoliposomes

The BR-CL, BR-PL, and BR-Lf nanoliposomes particle sizes were similar and narrowly distributed. The entrapment efficiency of BR nanoliposomes was more than 90%. The grafting ratio of Lf in BR-Lf was 65.9 ± 2.2% as shown in **Table 3**. Lf modification did not have much impact on particle size or entrapment efficiency of BR nanoliposomes. Microstructural observation showed that BR-CL, BR-PL, and BR-Lf were all quasi-circular unilamellar nanoliposomes with evident bilayer membranes (**Figure 1**). They were evenly distributed and their sizes were consistent with the particle size analysis.

Table 3 | **Particle size, PI, EE and Lf grafting ratio of BR nanoliposomes and DiR nanoliposomes**

	Particle size (nm)	PI (1 h)	EE (%)	Lfgrafted (%)
BR-CL	129.5±4.6	0.235±0.012	92.1±3.0	–
BR-PL	100.4±3.2	0.216±0.015	94.7±2.4	–
BR-Lf	118.6±4.5	0.246±0.017	90.4±1.2	65.9±2.2
DiR-CL	128.7±3.9	0.207±0.014	95.8±4.2	–
DiR-PL	105.2±4.1	0.212±0.015	97.2±3.6	–
DiR-Lf	120.6±3.5	0.228±0.013	96.5±2.9	66.2±3.8

BR: Berberine hydrochloride; BR-CL: BR common nanoliposomes; BR-Lf: BR PEGylated nanoliposomes with Lf modified; BR-PL: BR PEGylated nanoliposomes; CL: common blank nanoliposomes; DiR: 1,1′-dioctadecyl-3,3,3′,3′-tetramethyl-indotricarbocyanine iodide; DiR-CL: DiR common nanoliposomes; DiR-Lf: DiR PEGylated nanoliposomes with Lf modified; DiR-PL: DiR PEGylated nanoliposomes; EE: entrapment efficiency; Lf: lactoferrin; Lfgrafted: Lf grafting ratio; PI: performance index; PL: PEGylated blank nanoliposomes.

Lf improves brain targeting of BR nanoliposomes

In vivo fluorescence imaging was used to investigate the effect of Lf modification on the brain targeting capacity of BR nanoliposomes. During a 24-hour test period, fluorescence signals in the head, liver, and lung of mice in each liposome group initially increased and then decreased over time (**Figure 2A**). In the DiR-CL group, a high fluorescence signal in the liver and a very weak fluorescence signal in the head were observed just 2 hours after injection. In the DiR-PL group, a weak fluorescence signal was present in the brain 2 hours after injection, and the signal increased gradually until it reached the maximum at 8 hours. In the DiR-Lf group, the fluorescence signal in the brain was significantly higher than those in the DiR-CL and DiR-PL groups, and the high fluorescence signal was observed in the brain 2 hours after injection, indicating that the drug had reached the brain.

To confirm the *in vivo* imaging findings, we performed *ex vivo* mouse organ imaging (**Figure 2B** and **C**). Statistical analysis showed that there were significant differences between different preparations at the same time point and in the same preparation between different time points. The groups ordered by relative fluorescence intensity at each time point were DiR-Lf > DiR-PL > DiR-CL ($P < 0.01$), which was consistent with the *in vivo* imaging findings. The maximum fluorescence intensity of the DiR-Lf group at 4 hours was significantly higher than that of the DiR-PL group at 8 hours ($P < 0.01$).

BR-Lf improves behavioral capacity of a mouse model of AD-like Aβ neurotoxicity

The Y-maze test was used to determine the effects of different BR formulations on spatial recognition memory of the mouse model of AD-like Aβ neurotoxicity (**Figure 3A**). Compared with the sham group, the Aβ-injected model group had significantly reduced spontaneous alternation behavior ($P < 0.01$), suggesting that $A\beta_{1-42}$ induces working memory impairment and spatial memory impairment in mice. Spontaneous alternation behavior increased somewhat in the BR-S group and in the three different BR nanoliposomes groups compared with that in the model group. Spontaneous alternation behavior in the BR-S group did not significantly differ from that in the BR-CL group, but was decreased compared with that in the BR-PL ($P < 0.05$) and BR-Lf ($P < 0.01$) groups. Spontaneous alternation behavior in the BR-Lf group was significantly increased compared with that in the BR-S ($P < 0.01$) and BR-PL groups ($P < 0.05$).

In the novel object recognition test (**Figure 3B** and **C**), the groups had similar recognition times of the two identical objects, indicating that there were no group differences in preference to position of either object. The novel object preference indices at 1 and 24 hours in the model group were significantly decreased compared with those in the sham group ($P < 0.01$). There were no significant differences in novel object preference at 1 and 24 hours between the BR-S and BR-CL groups. The preference indices in the BR-PL ($P < 0.05$) and BR-Lf ($P < 0.01$) groups were significantly higher than those in the model group at both 1 and 24 hours. The preference index in the BR-Lf group was significantly higher than that in the BR-S ($P < 0.01$) and BR-PL ($P < 0.05$) groups at both 1 and 24 hours. These findings are consistent with the results of the spontaneous Y-maze alternation test.

BR-Lf inhibits AChE activity in hippocampal tissue of a mouse model of AD-like Aβ neurotoxicity

We assessed the effects of different BR formulations on AChE activity in hippocampal tissue of the mouse model of AD-like Aβ neurotoxicity (**Figure 4**). AChE activity in the mouse hippocampal tissue was markedly elevated in the model group compared with that in the sham group ($P < 0.01$). AChE activity was decreased to different degrees in the BR-S and BR nanoliposomes groups compared with that in the model group. AChE activity in the BR-Lf group was significantly decreased compared with that in the BR-S and BR-PL groups (both $P < 0.01$).

BR-Lf inhibits tau over-phosphorylation in the cerebral cortex of a mouse model of AD-like Aβ neurotoxicity

Immunohistochemistry results showed that the number of p-tau-positive cells in the cerebral cortex was higher in the model group than in the sham group ($P < 0.01$). The numbers of p-tau-positive cells in the BR-S group and BR nanoliposomes groups were decreased to different degrees compared with that in the model group (all $P < 0.01$). The number of p-tau-positive cells in the BR-Lf group was lower than that in the BR-PL group ($P < 0.01$) and that in the BR-S group ($P < 0.01$; **Figure 5**).

BR-Lf inhibits apoptosis in hippocampal tissue of a mouse model of AD-like Aβ neurotoxicity

Relative activity of caspase-3 and caspase-9 in the hippocampus of the model group were significantly increased compared with that in the sham group (both $P < 0.01$; **Figure 6**). Caspase-3 and caspase-9 activity in the hippocampus in the BR-S and BR nanoliposomes groups were decreased to different degrees, in particular in the BR-PL (both $P < 0.05$) and BR-Lf (both $P < 0.01$) groups, compared with those in the model group. Caspase-3 and caspase-9 activity in the BR-Lf group were significantly lower than those in the BR-PL group ($P < 0.01$ for caspase-3 and $P < 0.05$ for caspase-9).

Western blot assay was performed to determine the expression of apoptotic proteins Bax and Bcl-2 in the mouse hippocampal tissue (**Figure 7**). Bcl-2 protein expression was significantly decreased and Bax protein expression was significantly increased in the model group compared with the sham group (both $P < 0.01$). This finding suggests that $A\beta_{1-42}$ injection promotes apoptosis. Bcl-2 protein expression was significantly increased, and Bax protein expression was significantly decreased in the BR nanoliposomes groups ($P < 0.05$) compared with those in the model group. The increase in Bcl-2 expression in the BR-Lf group was significantly greater than the increase in the BR-PL group ($P < 0.05$). Bcl-2 expression was significantly increased and Bax expression was significantly decreased in the BR-Lf group compared with those in the BR-S group (both $P < 0.01$).

Discussion

In vivo fluorescence imaging has been increasingly applied in AD diagnosis and treatment and in *in vivo* tracing studies of anti-AD-targeting drug formulations because of ease in operation and rapid measurement (Lai et al., 2015; Dou et al., 2019). Lf modification enables accumulation of the carried drug in brain tissue, as detected by high fluorescence intensity and long residence time, in *in vivo* imaging studies, suggesting good brain-targeting specificity (Meng et al., 2018; Zhao et al., 2018). In this study, the fluorescence intensity of DiR-Lf was significantly increased compared with that of DiR-CL and DiR-PL in the brain, suggesting that DiR-Lf was transported across the BBB by the LfR, which greatly increases the brain-targeting capacity of the liposomes.

The Y-maze test was used to evaluate working memory capacity of the mice because it is easy to operate, poses minimal stress on animals, and yields reliable results (Faradila et al., 2020; Yang et al., 2022). BR-S at a low dose is characterized by rapid loss in blood circulation, and was therefore unable to significantly improve behavioral capacity of the mouse model of AD-like Aβ neurotoxicity (Wang et al., 2017). PEGylation of BR nanoliposomes extends the *in vivo* circulation time of the carried drug, so the clearance rates of BR in plasma and tissue are greatly reduced (Lin et al., 2013; Mo et al., 2018). This likely explains the markedly improved spontaneous alternation behavior and novel object preference index in the BR-PL group compared with those of the BR-S group. Previous studies have reported that LfR increased in the brain of people with neurodegenerative disorders, and have demonstrated that Lf-modified PEGylated liposomes bind to LfR at the BBB and are converted into positively-charged groups, which bind to the negatively-charged BBB under physiological conditions (Suzuki et al., 2005; Agrawal et al., 2017). LfR mediate specific one-way transport of Lf-carried drugs through differentiated BBB endothelial cells, without evident endothelial degradation (Fillebeen et al., 1999), so that drug concentration at the lesion site increases. In this study, the most significant improvement of behavioral capacity was observed in the BR-Lf group, likely because Lf increased brain targeting of the liposomes, consistent with the *in vivo* imaging results.

AD pathogenesis is related to serious deficiency of acetylcholine in the brain (Ferreira-Vieira et al., 2016). Inhibiting AChE activity to alleviate acetylcholine deficiency is an effective anti-AD strategy (Galimberti and Scarpini, 2016; Jiang et al., 2017). In the present study, each BR formulation inhibited AChE activity in hippocampal tissue in the mouse model of AD-like Aβ neurotoxicity, probably because favorable entropy increment promoted BR binding to AChE, and interaction between two types of molecules coupled with slight change in protein conformation led to lower enzymatic activity (Xiang et al., 2009). In a previous study, differences in the dosage form resulted in varied degrees of AChE inhibition; entrapment of BR by Lf-modified PEGylated liposomes greatly increased the concentration of BR reaching the brain, and an Lf-modified polymer or lipid drug carrier enabled a significant rise in BBB permeability of a neuroprotective drug (Ege, 2021), markedly elevating drug uptake in the brain (Gothwal et al., 2019). In the present study, BR-Lf provided the strongest AChE inhibition of all the nanoliposomes at the same dose.

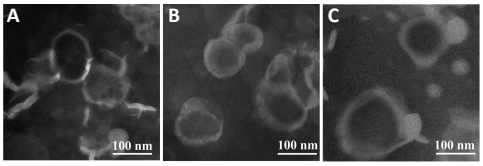

Figure 1 | Transmission electron microscope images of different BR nanoliposomes.
(A) BR-CL, (B) BR-PL, (C) BR-Lf. All of the nanoliposomes were quasi-circular unilamellar and evenly distributed. Scale bars: 100 nm. BR: Berberine hydrochloride; BR-CL: BR common nanoliposomes; BR-PL: BR PEGylated nanoliposomes; BR-Lf: BR PEGylated nanoliposomes with lactoferrin modified.

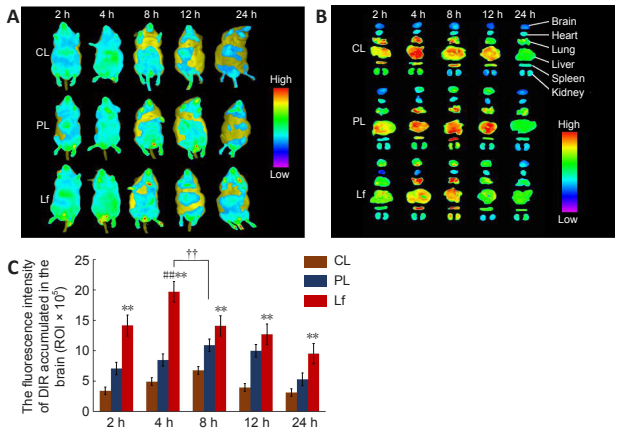

Figure 2 | Distribution of different DiR nanoliposomes in AD-like Aβ neurotoxicity model mice at different time points.
(A, B) *In vivo* (A) and *ex vivo* (B) fluorescence images in the brain of a mouse model of AD-like Aβ neurotoxicity. Fluorescence signal in the DiR-Lf group was significantly higher than that in the DiR-CL and DiR-PL groups. There was significant difference in fluorescence intensity between the DiR-CL, DiR-PL and DiR-Lf groups. (C) *Ex vivo* fluorescence intensity of different DiR nanoliposomes in the brain of a mouse model of AD-like Aβ neurotoxicity. Data are expressed as the mean ± SD (n = 3). $^{**}P < 0.01$, *vs.* DiR-CL group; $^{\#\#}P < 0.01$, *vs.* DiR-Lf group; $^{\dagger\dagger}P < 0.01$ (two-way analysis of variance followed by Duncan's multiple range test). AD: Alzheimer's disease; Aβ: amyloid-β protein; DiR: 1, 1′-dioctadecyl-3,3,3′,3′-tetramethyl-indotricarbocyanine iodide; DiR-CL (CL): DiR common nanoliposomes; DiR-Lf (Lf): DiR PEGylated nanoliposomes with lactoferrin modified; DiR-PL (PL): DiR PEGylated nanoliposomes.

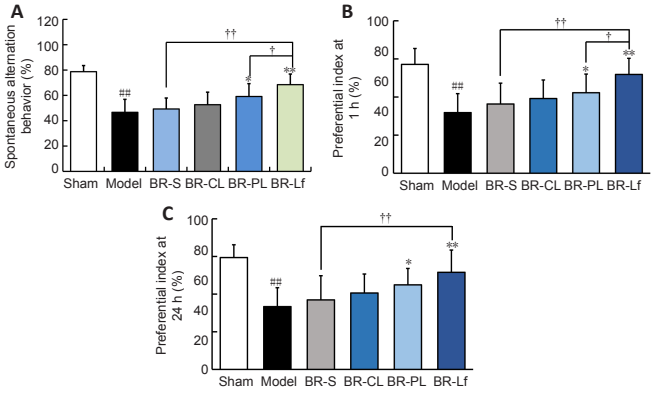

Figure 3 | Effects of different BR formulations on behavioral capacity tests in a mouse model of AD-like Aβ neurotoxicity.
(A) Spontaneous alternation behavior in the Y-maze test. (B, C) Novel object preference index at 1 (B) and 24 (C) hours. Data are expressed as mean ± SD (n = 9). $^{\#\#}P < 0.01$, *vs.* sham group; $^{*}P < 0.05$, $^{**}P < 0.01$, *vs.* model group; $^{\dagger}P < 0.05$, $^{\dagger\dagger}P < 0.01$ (one-way analysis of variance followed by the least significant difference *post hoc* test). AD: Alzheimer's disease; Aβ: amyloid-β protein; BR: berberine hydrochloride; BR-S: BR solution; BR-CL: BR common nanoliposomes; BR-PL: BR PEGylated nanoliposomes; BR-Lf: BR PEGylated nanoliposomes with lactoferrin modified.

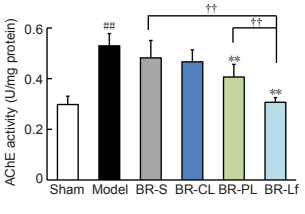

Figure 4 | Effects of different BR formulations on AChE activity in hippocampal tissue of a mouse model of AD-like Aβ neurotoxicity.
Data are expressed as the mean ± SD (n = 4). $^{\#\#}P < 0.01$, *vs.* sham group; $^{*}P < 0.05$, $^{**}P < 0.01$, *vs.* model group; $^{\dagger\dagger}P < 0.01$ (one-way analysis of variance followed by least significant difference *post hoc* test). AD: Alzheimer's disease; AChE: acetylcholinesterase; Aβ: amyloid-β protein; BR: berberine hydrochloride; BR-S: BR solution; BR-CL: BR common nanoliposomes; BR-PL: BR PEGylated nanoliposomes; BR-Lf: BR PEGylated nanoliposomes with lactoferrin modified.

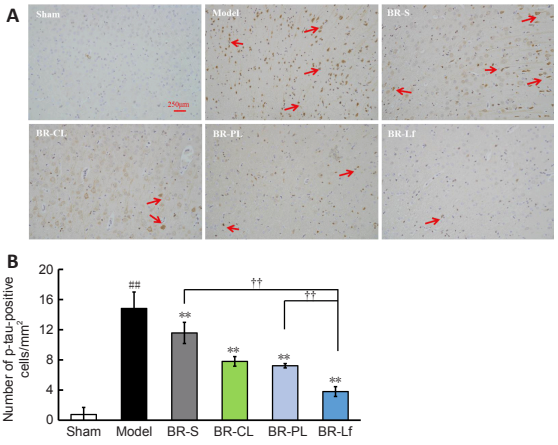

Figure 5 | Effects of different BR formulations on p-tau level in cerebral cortex of a mouse model of AD-like Aβ neurotoxicity.
(A) Immunohistochemistry images of different BR formulations on p-tau level of Ser396 (arrows) labeling in the cerebral cortex tissue of a mouse model of AD-like Aβ neurotoxicity. Of all of the groups, the BR-Lf group exhibited the optimal effects on the downregulation of hyperphosphorylated tau. Scale bars: 250 μm. (B) Quantitative analysis of p-tau-positive cells. Data are expressed as the mean ± SD (n = 4). $^{\#\#}P < 0.01$, *vs.* sham group; $^{**}P < 0.01$, *vs.* model group; $^{\dagger\dagger}P < 0.01$ (one-way analysis of variance followed by the least significant difference *post hoc* test). AD: Alzheimer's disease; Aβ: amyloid-β protein; BR: berberine hydrochloride; BR-S: BR solution; BR-CL: BR common nanoliposomes; BR-PL: BR PEGylated nanoliposomes; BR-Lf: BR PEGylated nanoliposomes with lactoferrin modified; p-Tau: Tau phosphorylation.

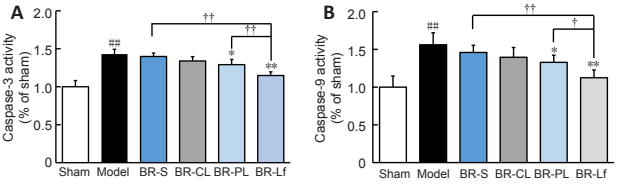

Figure 6 | Effects of different BR formulations on the relative activity of caspase-3 (A) and caspase-9 (B) in hippocampal tissue of a mouse model of AD-like Aβ neurotoxicity.
Data are expressed as the mean ± SD (n = 4). $^{\#\#}P < 0.01$, *vs.* sham group; $^{*}P < 0.05$, $^{**}P < 0.01$, *vs.* model group; $^{\dagger}P < 0.05$, $^{\dagger\dagger}P < 0.01$ (one-way analysis of variance followed by least significant difference *post hoc* test). AD: Alzheimer's disease; Aβ: amyloid β-protein; BR: berberine hydrochloride; BR-S: BR solution; BR-CL: BR common nanoliposomes; BR-PL: BR PEGylated nanoliposomes; BR-Lf: BR PEGylated nanoliposomes with lactoferrin modified.

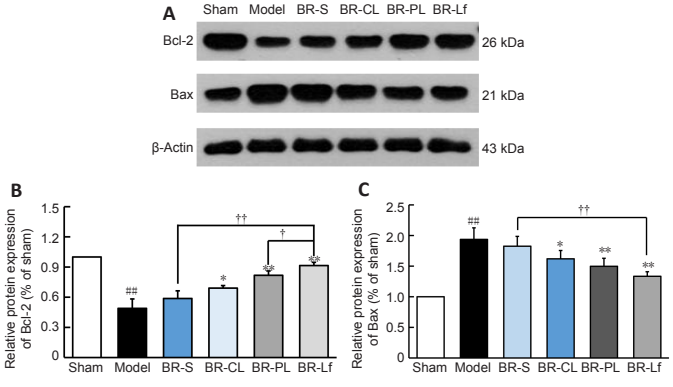

Figure 7 | Effects of different BR formulations on expression levels of apoptotic proteins Bax and Bcl-2 in hippocampal tissue of a mouse model of AD-like Aβ neurotoxicity.
(A) Western blotting of Bax and Bcl-2. β-Actin was an internal reference. (B, C) Quantitative results of relative expression levels of apoptotic proteins Bcl-2 (B) and Bax (C). Data are expressed as the mean ± SD (n = 3). $^{\#\#}P < 0.01$, *vs.* sham group; $^{*}P < 0.05$, $^{**}P < 0.01$, *vs.* model group; $^{\dagger}P < 0.05$, $^{\dagger\dagger}P < 0.01$ (one-way analysis of variance followed by LSD *post hoc* test). AD: Alzheimer's disease; Aβ: amyloid-β protein; BR: berberine hydrochloride; BR-S: BR solution; BR-CL: BR common nanoliposomes; BR-PL: BR PEGylated nanoliposomes; BR-Lf: BR PEGylated nanoliposomes with lactoferrin modified.

Tau is a microtubule-associated protein capable of promoting neuronal microtubule cytoskeleton assembly and maintaining microtubule stability (Duan et al., 2012). In the brain of an AD patient, each tau molecule has two to six more phosphoric groups than in people without AD; over-phosphorylation of tau promotes microtubule disintegration, and the microtubules pair with other phosphorylated tau protein molecules to form paired helical filaments that aggregate into neurofibrillary tangles, leading to neuronal apoptosis (Bazrgar et al., 2020). In this study, BR-S and BR nanoliposomes inhibited p-tau at Ser396 in the mouse hippocampal tissue to variable extents, perhaps because BR reduced tau over-phosphorylation by activating protein phosphatase 2A and inhibiting activity of protein phosphokinase (Liu et al., 2005; Takashima, 2006). A previous study has proposed that by inhibiting the nuclear factor kappa-B signaling pathway activation and neuroinflammatory responses, BR reduces tau over-phosphorylation to alleviate cognitive symptoms in AD model mice (He et al., 2017). In this study, BR-Lf greatly reduced tau over-phosphorylation at Ser396 and improved working memory and new object recognition in the mouse model of AD-like Aβ neurotoxicity, which is consistent with the above findings.

Anti-apoptotic Bcl-2 and pro-apoptotic Bax are antagonistic proteins; Bcl-2 and Bax can form a dimer to inactivate Bax, and the Bcl-2/Bax ratio is closely related to apoptosis, dictating the level of activation of pro-apoptotic factor caspase-3 (Croker et al., 2011). Caspase-3 is directly involved in the cleavage of Aβ and tau protein and induces apoptosis, and its expression level directly reflects the apoptosis level (Chu et al., 2017). In this study, BR-Lf reversed the changes in Bcl-2 and Bax expression to greatly reduce caspase-3 and caspase-9 activity, suggesting that BR-Lf modulates Bcl-2 and Bax expression to inhibit abnormal apoptosis of hippocampal neurons and alleviate neuronal damage in model mice (Huang et al., 2017). In this apoptosis-inhibiting effect, BR-Lf was superior to BR-S, BR-CL, and BR-PL, indicating that the Lf-modified PEGylated lipid carrier increases BR concentration in the brain and potentiates the neuroprotective effects.

There were some limitations to this study. We did not determine whether the neuroprotective effects of BR-Lf in a mouse model of AD-like Aβ neurotoxicity were dose-dependent. Further, we did not compare between different administration methods. More systematic research is needed, such as investigation of synaptic and postsynaptic markers and gliosis. We will investigate the neuroprotective ability of BR-Lf with different administration methods and doses in future research.

In conclusion, we successfully prepared Lf-modified PEGylated BR nanoliposomes and demonstrated that the modification potentiated the anti-AD effect of BR. Lf modification improved the brain-targeting and neuroprotective effects of BR nanoliposomes. BR-Lf improved the behavioral capacity of a mouse model of AD-like Aβ neurotoxicity induced by $A\beta_{1-42}$ through inhibiting AChE activity, antagonizing tau over-phosphorylation, and inhibiting neuronal apoptosis. The findings suggest that BR-Lf is a promising anti-AD formulation.

Author contributions: *Study conception and design: KJC, ZZW, LW, BQZ, WHC, YHL; experiment implementation and data analysis: LW, QQJ; manuscript draft: LW. All authors read and approved the final manuscript.*
Conflicts of interest: *The authors declare no conflicts of interest.*

References

Agrawal M, Ajazuddin, Tripathi DK, Saraf S, Saraf S, Antimisiaris SG, Mourtas S, Hammarlund-Udenaes M, Alexander A (2017) Recent advancements in liposomes targeting strategies to cross blood-brain barrier (BBB) for the treatment of Alzheimer's disease. J Control Release 260:61-77.

Allijn IE, Czarny BMS, Wang X, Chong SY, Weiler M, da Silva AE, Metselaar JM, Lam CSP, Pastorin G, de Kleijn DPV, Storm G, Wang JW, Schiffelers RM (2017) Liposome encapsulated berberine treatment attenuates cardiac dysfunction after myocardial infarction. J Control Release 247:127-133.

Bai D, Jin G, Zhang D, Zhao L, Wang M, Zhu Q, Zhu L, Sun Y, Liu X, Chen X, Zhang L, Li W, Cui Y (2019) Natural silibinin modulates amyloid precursor protein processing and amyloid-β protein clearance in APP/PS1 mice. J Physiol Sci 69:643-652.

Ballard C, Aarsland D, Cummings J, O'Brien J, Mills R, Molinuevo JL, Fladby T, Williams G, Doherty P, Corbett A, Sultana J (2020) Drug repositioning and repurposing for Alzheimer disease. Nat Rev Neurol 16:661-673.

Bazrgar M, Khodabakhsh P, Mohagheghi F, Prudencio M, Ahmadiani A (2020) Brain microRNAs dysregulation: Implication for missplicing and abnormal post-translational modifications of tau protein in Alzheimer's disease and related tauopathies. Pharmacol Res 155:104729.

Cai XX, Lü YN, Qi Y (2022) Long-circulating lipsomes: application and mechanism. Zhongguo Zuzhi Gongcheng Yanjiu 26:2613-2617.

Calvo A, Moreno E, Larrea E, Sanmartín C, Irache JM, Espuelas S (2020) Berberine-loaded liposomes for the treatment of leishmania infantum-infected BALB/c Mice. Pharmaceutics 12:858.

Chen Q, Mo R, Wu N, Zou X, Shi C, Gong J, Li J, Fang K, Wang D, Yang D, Wang K, Chen J (2017) Berberine ameliorates diabetes-associated cognitive decline through modulation of aberrant inflammation response and insulin signaling pathway in DM rats. Front Pharmacol 8:334.

Chu J, Lauretti E, Praticò D (2017) Caspase-3-dependent cleavage of Akt modulates tau phosphorylation via GSK3β kinase: implications for Alzheimer's disease. Mol Psychiatry 22:1002-1008.

Croker BA, O'Donnell JA, Nowell CJ, Metcalf D, Dewson G, Campbell KJ, Rogers KL, Hu Y, Smyth GK, Zhang JG, White M, Lackovic K, Cengia LH, O'Reilly LA, Bouillet P, Cory S, Strasser A, Roberts AW (2011) Fas-mediated neutrophil apoptosis is accelerated by Bid, Bak, and Bax and inhibited by Bcl-2 and Mcl-1. Proc Natl Acad Sci U S A 108:13135-13140.

Cummings J (2021) Drug development for psychotropic, cognitive-enhancing, and disease-modifying treatments for alzheimer's disease. J Neuropsychiatry Clin Neurosci 33:3-13.

Cummings J, Lee G, Ritter A, Sabbagh M, Zhong K (2020) Alzheimer's disease drug development pipeline: 2020. Alzheimers Dement (N Y) 6:e12050.

de Oliveira JS, Abdalla FH, Dornelles GL, Adefegha SA, Palma TV, Signor C, da Silva Bernardi J, Baldissarelli J, Lenz LS, Magni LP, Rubin MA, Pillat MM, de Andrade CM (2016) Berberine protects against memory impairment and anxiogenic-like behavior in rats submitted to sporadic Alzheimer's-like dementia: Involvement of acetylcholinesterase and cell death. Neurotoxicology 57:241-250.

Dou WT, Zhang JJ, Li Q, Guo Z, Zhu W, Chen GR, Zhang HY, He XP (2019) Fluorescence imaging of Alzheimer's disease with a flat ensemble formed between a quinoline-malononitrile AIEgen and thin-layer molybdenum disulfide. Chembiochem 20:1856-1860.

Duan Y, Dong S, Gu F, Hu Y, Zhao Z (2012) Advances in the pathogenesis of Alzheimer's disease: focusing on tau-mediated neurodegeneration. Transl Neurodegener 1:24.

Durairajan SS, Liu LF, Lu JH, Chen LL, Yuan Q, Chung SK, Huang L, Li XS, Huang JD, Li M (2012) Berberine ameliorates β-amyloid pathology, gliosis, and cognitive impairment in an Alzheimer's disease transgenic mouse model. Neurobiol Aging 33:2903-2919.

Ege D (2021) Action mechanisms of curcumin in alzheimer's disease and its brain targeted delivery. Materials (Basel) 14:3332.

Faradila F, Syafrita Y, Lipoeto NI (2020) Relationship between amyloid-beta 42 levels and y-maze alternation values in sprague dawley Alzheimer's induction received medium-chain triglycerides therapy. Open Access Maced J Med Sci 8:476-480.

Ferreira-Vieira TH, Guimaraes IM, Silva FR, Ribeiro FM (2016) Alzheimer's disease: targeting the cholinergic system. Curr Neuropharmacol 14:101-115.

Fillebeen C, Descamps L, Dehouck MP, Fenart L, Benaïssa M, Spik G, Cecchelli R, Pierce A (1999) Receptor-mediated transcytosis of lactoferrin through the blood-brain barrier. J Biol Chem 274:7011-7017.

Galimberti D, Scarpini E (2016) Old and new acetylcholinesterase inhibitors for Alzheimer's disease. Expert Opin Investig Drugs 25:1181-1187.

Gong CX, Liu F, Grundke-Iqbal I, Iqbal K (2006) Dysregulation of protein phosphorylation/dephosphorylation in Alzheimer's disease: a therapeutic target. J Biomed Biotechnol 2006:31825.

Gopalan D, Pandey A, Udupa N, Mutalik S (2020) Receptor specific, stimuli responsive and subcellular targeted approaches for effective therapy of Alzheimer: role of surface engineered nanocarriers. J Control Release 319:183-200.

Goswami P, Afjal MA, Akhter J, Mangla A, Khan J, Parvez S, Raisuddin S (2020) Involvement of endoplasmic reticulum stress in amyloid β ((1-42))-induced Alzheimer's like neuropathological process in rat brain. Brain Res Bull 165:108-117.

Gothwal A, Kumar H, Nakhate KT, Ajazuddin, Dutta A, Borah A, Gupta U (2019) Lactoferrin coupled lower generation PAMAM Dendrimers for brain targeted delivery of memantine in aluminum-chloride-induced Alzheimer's disease in mice. Bioconjug Chem 30:2573-2583.

Han XX, Xie Y, Zhao B, Ozaki Y (2010) Highly sensitive protein concentration assay over a wide range via surface-enhanced Raman scattering of Coomassie brilliant blue. Anal Chem 82:4325-4328.

He W, Wang C, Chen Y, He Y, Cai Z (2017) Berberine attenuates cognitive impairment and ameliorates tau hyperphosphorylation by limiting the self-perpetuating pathogenic cycle between NF-κB signaling, oxidative stress and neuroinflammation. Pharmacol Rep 69:1341-1348.

Hernandez C, Shukla S (2022) Liposome based drug delivery as a potential treatment option for Alzheimer's disease. Neural Regen Res 17:1190-1198.

Huang FY, Chen WJ, Lee WY, Lo ST, Lee TW, Lo JM (2013) In vitro and in vivo evaluation of lactoferrin-conjugated liposomes as a novel carrier to improve the brain delivery. Int J Mol Sci 14:2862-2874.

Huang M, Jiang X, Liang Y, Liu Q, Chen S, Guo Y (2017) Berberine improves cognitive impairment by promoting autophagic clearance and inhibiting production of β-amyloid in APP/tau/PS1 mouse model of Alzheimer's disease. Exp Gerontol 91:25-33.

Huang RQ, Ke WL, Qu YH, Zhu JH, Pei YY, Jiang C (2007) Characterization of lactoferrin receptor in brain endothelial capillary cells and mouse brain. J Biomed Sci 14:121-128.

Imenshahidi M, Hosseinzadeh H (2020) Chapter 14- Berberine neuroprotection and antioxidant activity. In: Oxidative Stress and Dietary Antioxidants in Neurological Diseases (Martin CR, Preedy VR, eds), pp 199-216: Academic Press.

Jaafar-Maalej C, Diab R, Andrieu V, Elaissari A, Fessi H (2010) Ethanol injection method for hydrophilic and lipophilic drug-loaded liposome preparation. J Liposome Res 20:228-243.

Ji XF, Chi TY, Xu Q, He XL, Zhou XY, Zhang R, Zou LB (2014) Xanthoceraside ameliorates mitochondrial dysfunction contributing to the improvement of learning and memory impairment in mice with intracerebroventricular injection of aβ1-42. Evid Based Complement Alternat Med 2014:969342.

Jiang Y, Gao H, Turdu G (2017) Traditional Chinese medicinal herbs as potential AChE inhibitors for anti-Alzheimer's disease: A review. Bioorg Chem 75:50-61.

Jin G, Bai D, Yin S, Yang Z, Zou D, Zhang Z, Li X, Sun Y, Zhu Q (2016) Silibinin rescues learning and memory deficits by attenuating microglia activation and preventing neuroinflammatory reactions in SAMP8 mice. Neurosci Lett 629:256-261.

Karami Z, Saghatchi Zanjani MR, Rezaee S, Rostamizadeh K, Hamidi M (2019) Neuropharmacokinetic evaluation of lactoferrin-treated indinavir-loaded nanoemulsions: remarkable brain delivery enhancement. Drug Dev Ind Pharm 45:736-744.

Lai L, Zhao C, Su M, Ye J, Jiang H, Wang X (2015) In vivo rapid fluorescence imaging of Alzheimer's disease through accurate target bio-marking of zinc gluconate. Sci Bull (Beijing) 60:1465-1467.

Lin YC, Kuo JY, Hsu CC, Tsai WC, Li WC, Yu MC, Wen HW (2013) Optimizing manufacture of liposomal berberine with evaluation of its antihepatoma effects in a murine xenograft model. Int J Pharm 441:381-388.

Liu F, Grundke-Iqbal I, Iqbal K, Gong CX (2005) Contributions of protein phosphatases PP1, PP2A, PP2B and PP5 to the regulation of tau phosphorylation. Eur J Neurosci 22:1942-1950.

Liu S, Zhang SM, Ju RJ, Xiao Y, Wang X, Song XL, Gu LY, Cheng L, Li XT, Chen GR (2017) Antitumor efficacy of Lf modified daunorubicin plus honokiol liposomes in treatment of brain glioma. Eur J Pharm Sci 106:185-197.

Luo X, Li J, Guo L, Cheng X, Zhang T, Deng Y (2013) Preparation of berberine hydrochloride long-circulating liposomes by ionophore A23187-mediated ZnSO4 gradient method. Asian J Pharm Sci 8:261-266.

Meng Q, Wang A, Hua H, Jiang Y, Wang Y, Mu H, Wu Z, Sun K (2018) Intranasal delivery of Huperzine A to the brain using lactoferrin-conjugated N-trimethylated chitosan surface-modified PLGA nanoparticles for treatment of Alzheimer's disease. Int J Nanomedicine 13:705-718.

Mirhadi E, Rezaee M, Malaekeh-Nikouei B (2018) Nano strategies for berberine delivery, a natural alkaloid of Berberis. Biomed Pharmacother 104:465-473.

Mittal S, Ashhar MU, Qizilbash FF, Qamar Z, Narang JK, Kumar S, Ali J, Baboota S (2020) Ligand conjugated targeted nanotherapeutics for treatment of neurological disorders. Curr Pharm Des 26:2291-2305.

Mo L, Song JG, Lee H, Zhao M, Kim HY, Lee YJ, Ko HW, Han HK (2018) PEGylated hyaluronic acid-coated liposome for enhanced in vivo efficacy of sorafenib via active tumor cell targeting and prolonged systemic exposure. Nanomedicine 14:557-567.

Pattni BS, Chupin VV, Torchilin VP (2015) New developments in liposomal drug delivery. Chem Rev 115:10938-10966.

Percie du Sert N, Hurst V, Ahluwalia A, Alam S, Avey MT, Baker M, Browne WJ, Clark A, Cuthill IC, Dirnagl U, Emerson M, Garner P, Holgate ST, Howells DW, Karp NA, Lazic SE, Lidster K, MacCallum CJ, Macleod M, Pearl EJ, et al. (2020) The ARRIVE guidelines 2.0: Updated guidelines for reporting animal research. PLoS Biol 18:e3000410.

Rahimi-Madiseh M, Lorigoini Z, Zamani-Gharaghoshi H, Rafieian-Kopaei M (2017) Berberis vulgaris: specifications and traditional uses. Iran J Basic Med Sci 20:569-587.

Raju M, Kulkarni YA, Wairkar S (2019) Therapeutic potential and recent delivery systems of berberine: A wonder molecule. J Funct Foods 61:103517.

Sadraie S, Kiasalari Z, Razavian M, Azimi S, Sedighnejad L, Afshin-Majd S, Baluchnejadmojarad T, Roghani M (2019) Berberine ameliorates lipopolysaccharide-induced learning and memory deficit in the rat: insights into underlying molecular mechanisms. Metab Brain Dis 34:245-255.

Schneider CA, Rasband WS, Eliceiri KW (2012) NIH Image to ImageJ: 25 years of image analysis. Nat Methods 9:671-675.

Shanbhag SM, Kulkarni HJ, Gaitonde BB (1970) Pharmacological actions of berberine on the central nervous system. Jpn J Pharmacol 20:482-487.

Song D, Hao J, Fan D (2020) Biological properties and clinical applications of berberine. Front Med 14:564-582.

Suzuki YA, Lopez V, Lönnerdal B (2005) Mammalian lactoferrin receptors: structure and function. Cell Mol Life Sci 62:2560-2575.

Takashima A (2006) GSK-3 is essential in the pathogenesis of Alzheimer's disease. J Alzheimers Dis 9:309-317.

Tang Y, Min Z, Xiang XJ, Liu L, Ma YL, Zhu BL, Song L, Tang J, Deng XJ, Yan Z, Chen GJ (2018) Estrogen-related receptor alpha is involved in Alzheimer's disease-like pathology. Exp Neurol 305:89-96.

Wang SS, Zhang Z, Zhang X, Long Q, He WB, Chen NH (2018) Advances in immunotherapy of Alzheimer's disease with traditional Chinese medicine. Yao Xue Xue Bao 53:1023-1029.

Wang X, Wang Q, Liu Z, Zheng X (2017) Preparation, pharmacokinetics and tumour-suppressive activity of berberine liposomes. J Pharm Pharmacol 69:625-632.

Xiang J, Yu C, Yang F, Yang L, Ding H (2009) Conformation-activity studies on the interaction of berberine with acetylcholinesterase: Physical chemistry approach. Progr Nat Sci 19:1721-1725.

Yan X, Xu L, Bi C, Duan D, Chu L, Yu X, Wu Z, Wang A, Sun K (2018) Lactoferrin-modified rotigotine nanoparticles for enhanced nose-to-brain delivery: LESA-MS/MS-based drug biodistribution, pharmacodynamics, and neuroprotective effects. Int J Nanomedicine 13:273-281.

Yang GZ, Gao QC, Li WR, Cai HY, Zhao HM, Wang JJ, Zhao XR, Wang JX, Wu MN, Zhang J, Hölscher C, Qi JS, Wang ZJ (2022) (D-Ser2) oxyntomodulin recovers hippocampal synaptic structure and theta rhythm in Alzheimer's disease transgenic mice. Neural Regen Res 17:2072-2078.

Yuan NN, Cai CZ, Wu MY, Su HX, Li M, Lu JH (2019) Neuroprotective effects of berberine in animal models of Alzheimer's disease: a systematic review of pre-clinical studies. BMC Complement Altern Med 19:109.

Zhang Y, Huang NQ, Yan F, Jin H, Zhou SY, Shi JS, Jin F (2018) Diabetes mellitus and Alzheimer's disease: GSK-3β as a potential link. Behav Brain Res 339:57-65.

Zhao C, Zhang J, Hu H, Qiao M, Chen D, Zhao X, Yang C (2018) Design of lactoferrin modified lipid nano-carriers for efficient brain-targeted delivery of nimodipine. Mater Sci Eng C Mater Biol Appl 92:1031-1040.

C-Editor: Zhao M; S-Editors: Yu J, Li CH; L-Editors: McCpllum L, Song LP; T-Editor: Jia Y